

3-1-2000

## Fast integral methods for conformal antenna and array modeling in conjunction with hybrid finite element formulations

John L. Volakis  
*University of Michigan, Ann Arbor*

Thomas F. Eibert  
*University of Michigan, Ann Arbor*

Kubilay Sertel  
*University of Michigan, Ann Arbor*

Follow this and additional works at: [https://digitalcommons.fiu.edu/ece\\_fac](https://digitalcommons.fiu.edu/ece_fac)

---

### Recommended Citation

Volakis, John L.; Eibert, Thomas F.; and Sertel, Kubilay, "Fast integral methods for conformal antenna and array modeling in conjunction with hybrid finite element formulations" (2000). *Electrical and Computer Engineering Faculty Publications*. 82.

[https://digitalcommons.fiu.edu/ece\\_fac/82](https://digitalcommons.fiu.edu/ece_fac/82)

This work is brought to you for free and open access by the College of Engineering and Computing at FIU Digital Commons. It has been accepted for inclusion in Electrical and Computer Engineering Faculty Publications by an authorized administrator of FIU Digital Commons. For more information, please contact [dcc@fiu.edu](mailto:dcc@fiu.edu).

# Fast integral methods for conformal antenna and array modeling in conjunction with hybrid finite element formulations

John L. Volakis, Thomas F. Eibert, and Kubilay Sertel

Radiation Laboratory, Department of Electrical Engineering and Computer Science  
University of Michigan, Ann Arbor

**Abstract.** Fast integral methods are used to improve the efficiency of hybrid finite element formulations for conformal antenna and array modeling. We consider here cavity-backed configurations recessed in planar and curved ground planes as well as infinite periodic structures with boundary integral (BI) terminations on the top and bottom bounding surfaces. Volume tessellation is based on triangular prismatic elements which are well suited for layered structures and still give the required modeling flexibility for irregular antenna and array elements. For planar BI terminations of finite and infinite arrays the adaptive integral method is used to achieve  $\mathcal{O}(N \log N)$  computational complexity in evaluating the matrix-vector products within the iterative solver. In the case of curved mesh truncations for finite arrays the fast multipole method is applied to obtain  $\mathcal{O}(N^{1.5})$  complexity for the evaluation of the matrix-vector products. Advantages and disadvantages of these methods as they relate to different applications are discussed, and numerical results are provided.

## 1. Introduction

Hybrid finite element boundary integral (FE/BI) methods have been widely applied for analysis of conformal antennas and arrays [Volakis *et al.*, 1997; Volakis *et al.*, 1998]. Because of requirements for accuracy, full volumetric materials characterization, accurate feed modeling, and structural complexity, the FE method is one of the most attractive simulation approaches that combines rigor and adaptability. Nevertheless, these attributes are often not sufficient for practical characterization of complex antenna apertures and arrays due to CPU time and memory requirements associated with the BI portion of the hybrid FE/BI system. The BI subsystem dominates the CPU requirements with its  $\mathcal{O}(N^2)$  computations, where  $N$  refers to the number of unknowns on the antenna/array aperture. However, recent developments on fast integral methods have allowed us to circumvent some of these CPU bottlenecks and are permitting the analysis of large finite apertures

and multilayered arrays. Eventually, these speedups can lead to algorithms which can be used for design purposes.

Fast integral methods are typically used in connection with iterative solvers, and their aim is to speed up the matrix-vector product calculations, the most time consuming step in any iterative algorithm such as the conjugate gradient (CG), biconjugate gradient (BiCG), quasi-minimal residual (QMR), and the generalized minimal residual (GMRES) routines [Saad, 1996]. Fast methods are often referred to as matrix compression algorithms, and  $k$ -space methods [Bojarski, 1971] were among the first such approaches to be used with iterative solvers. Although  $k$ -space methods lead to  $\mathcal{O}(N \log N)$  memory and computational complexity, their application is restricted to systems/geometries which can be approximated with circulant matrices. Originally, this requirement could only be fulfilled using uniform discretizations of the integral equation. However, recently introduced fast integral methods such as the fast multipole method (FMM) [Coifman *et al.*, 1993; Bindiganavale and Volakis, 1997; Lu and Jin, 1996; Chew *et al.*, 1997; Song *et al.*, 1997; Sheng *et al.*, 1998] and the adaptive integral method (AIM) [Bles-

Copyright 2000 by the American Geophysical Union.

Paper number 1999RS900050.  
0048-6604/00/1999RS900050\$11.00

*zynski et al.*, 1996; *Anastassiou et al.*, 1998; *Bindiganavale and Volakis*, 1998; *Eibert and Volakis*, 1999] are rid of restrictions for uniform discretization of the original geometries. These methods have been shown to deliver memory and CPU reduction down to  $\mathcal{O}(N^{1.5})$  or better. Windowed FMM [*Burkholder and Kwon*, 1996] and multilevel FMM [*Song et al.*, 1997] can reduce CPU down to  $\mathcal{O}(N^{1.33})$  or even  $\mathcal{O}(N \log N)$ . Early electromagnetic applications of FMM concentrated on pure integral equation approaches, but uses of FMM in the context of hybrid FE/BI formulations have also been reported [*Lu and Jin*, 1996; *Sheng et al.*, 1998]. AIM can be considered as the natural extension of the  $k$ -space methods and was introduced for arbitrary surface and volumetric scattering problems [*Bleszynski et al.*, 1996] and is especially the method of choice for planar BI surfaces. In this case, only two-dimensional fast Fourier transform (FFT) algorithms need to be used, and the method results in low  $\mathcal{O}(N \log N)$  complexity. Thus the speedup of AIM is considerably better than that of FMM or multilevel FMM for planar boundaries even for relatively small numbers of unknowns. Recent pure integral equation applications of AIM [*Bleszynski et al.*, 1996; *Anastassiou et al.*, 1998] and hybrid FE/BI implementations of AIM [*Bindiganavale and Volakis*, 1998; *Eibert and Volakis*, 1999] have verified its superior speedup and accuracy for planar BI treatments.

In this paper we consider hybrid FE/BI formulations for cavity-backed configurations recessed in

planar and curved ground planes. In contrast to previous works, the emphasis of this paper is on the application of fast methods to infinite periodic and finite arrays and frequency selective radomes. For planar BI truncations of infinite arrays, AIM is used to speed up the BI, whereas FMM is used to increase the efficiency of curved BI terminations. In this context the main differences of FMM and AIM will be discussed together with the inherent approximations of each technique. Numerical results are shown for conformal printed antennas and frequency selective surfaces (FSSs).

## 2. Hybrid FE/BI formulation

The hybrid FE/BI formulation for cavity-backed antennas recessed in a ground plane has been given by *Volakis et al.* [1997,1998], whereas periodic array modeling has been discussed extensively by *Lucas and Fontana* [1995], *McGrath and Pyati* [1996], and *Eibert et al.* [1999]. Below we briefly present a unified formulation, where the differences between single elements and infinite periodic arrays are in the Green's function and in the necessity to apply periodic boundary conditions (PBCs) at the volume and surface boundaries. The latter allows the reduction of the computational domain to a single periodic cell. In the context of hybrid FE/BI formulation, the resulting system of equations for the antenna/array structure illustrated in Figure 1 is of the form

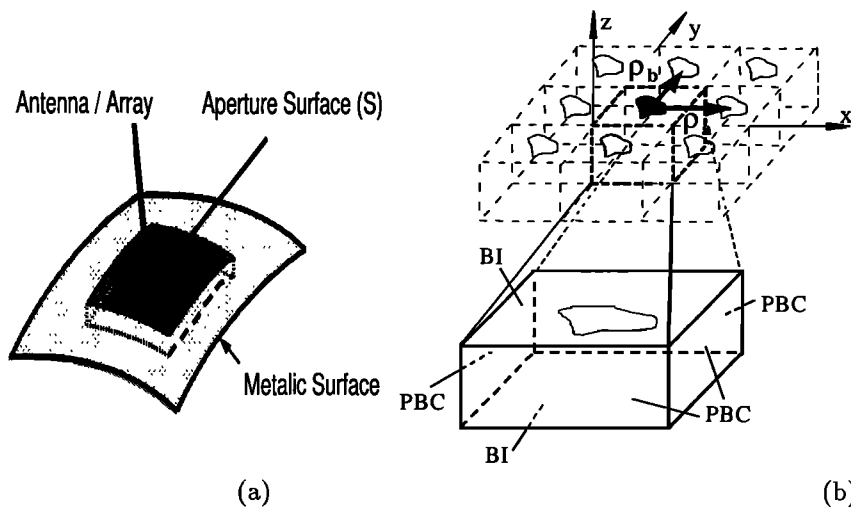


Figure 1. (a) Finite array in the cavity, and (b) infinite periodic structure.

$$[\mathcal{A}] \begin{Bmatrix} \{E^V\} \\ \{E^S\} \end{Bmatrix} + \begin{bmatrix} [0] & [0] \\ [0] & [\mathcal{B}] \end{bmatrix} \times \begin{Bmatrix} \{E^V\} \\ \{E^S\} \end{Bmatrix} = \begin{Bmatrix} \{b^V\} \\ \{b^S\} \end{Bmatrix}. \quad (1)$$

Here  $\{E^V\}$  denotes the electric field unknowns within the volume enclosed by  $S$ , whereas  $\{E^S\}$  represents the corresponding unknowns on the boundary  $S$ . The matrix  $[\mathcal{A}]$  is sparse and is associated with the finite element volume discretization, whereas  $[\mathcal{B}]$  stands for the fully populated BI system. The latter is obtained from a discretization of the surface integral equation for the magnetic field intensity  $\mathbf{H}$

$$\begin{aligned} \mathbf{H} &= -j \frac{k}{Z} \left[ \iint_S g(\mathbf{r}, \mathbf{r}') (\mathbf{E} \times \hat{\mathbf{n}}) ds \right. \\ &+ \left. \frac{1}{k^2} \nabla \iint_S g(\mathbf{r}, \mathbf{r}') \nabla' \cdot (\mathbf{E} \times \hat{\mathbf{n}}) ds \right] \\ &+ \mathbf{H}^{\text{inc}}, \end{aligned} \quad (2)$$

in which  $\mathbf{H}^{\text{inc}}$  is an externally incident electromagnetic wave,  $g(\mathbf{r}, \mathbf{r}') = e^{-jk|\mathbf{r}-\mathbf{r}'|}/(2\pi|\mathbf{r}-\mathbf{r}'|)$  is the scalar Green's function for a magnetic current element over a ground plane, and  $k$  and  $Z$  are the free-space wave number and wave impedance, respectively. The same half-space Green's function is used to obtain an approximate solution when the antenna/array is on a slightly curved surface. The excitation column  $\{b^V\}$  is due to internal antenna sources, and  $\{b^S\}$  refers to the external incident field excitations  $\mathbf{H}^{\text{inc}}$  (for scattering computations). When the above system refers to cavity-backed antennas or finite arrays in a cavity-backed configuration, the boundary condition on the vertical/side walls of the cavity is simply  $\hat{\mathbf{n}} \times \mathbf{E} = 0$ . Triangular prismatic elements [Özdemir and Volakis, 1997; Graglia et al., 1998] are used to discretize the volume. The associated basis functions on the aperture then become the Rao-Wilton-Glisson surface elements, and these are used to construct the BI submatrix.

Infinite periodic arrays are assumed to be periodic in the  $xy$  plane, and the  $(m, n)$ th cell of the array is obtained by shifting the  $(0, 0)$ th cell through the relation

$$\boldsymbol{\rho}_{mn} = m \boldsymbol{\rho}_a + n \boldsymbol{\rho}_b. \quad (3)$$

Here  $\boldsymbol{\rho}_a, \boldsymbol{\rho}_b$  are the lattice vectors in the  $xy$  plane, and (3) is only valid for planar periodic structures. Clearly, for curved arrays the complete array geometry needs to be considered since a periodicity cannot be defined by an equation similar to (3). For periodic excitation of the array with a linear phase factor, the fields in the array obey the periodicity conditions

$$\mathbf{E}(\mathbf{r} + m\boldsymbol{\rho}_a + n\boldsymbol{\rho}_b) = \mathbf{E}(\mathbf{r})e^{-j\mathbf{k}_{t00} \cdot (m\boldsymbol{\rho}_a + n\boldsymbol{\rho}_b)}, \quad (4)$$

$$\mathbf{H}(\mathbf{r} + m\boldsymbol{\rho}_a + n\boldsymbol{\rho}_b) = \mathbf{H}(\mathbf{r})e^{-j\mathbf{k}_{t00} \cdot (m\boldsymbol{\rho}_a + n\boldsymbol{\rho}_b)}$$

where

$$\begin{aligned} \mathbf{k}_{t00} &= k_{x00} \hat{\mathbf{x}} + k_{y00} \hat{\mathbf{y}} \\ &= k \sin \vartheta_0 \cos \varphi_0 \hat{\mathbf{x}} + k \sin \vartheta_0 \sin \varphi_0 \hat{\mathbf{y}} \end{aligned} \quad (5)$$

with  $\vartheta_0, \varphi_0$  describing the scan direction of the array or the propagation direction of an incident plane wave. Using this periodicity condition and the BI representation in (2), the computational domain can be reduced to a single unit cell of the array [Lucas and Fontana, 1995; McGrath and Pyati, 1996; Eibert et al., 1999] (see Figure 1). This also implies that  $g(\mathbf{r}, \mathbf{r}')$  in (2) must be replaced by the appropriate periodic Green's function and the PBCs must be explicitly enforced on the vertical side walls of the unit cell mesh. Many periodic BI implementations utilize spectral domain formulations [Lucas and Fontana, 1995; McGrath and Pyati, 1996]. However, here we use a spatial domain approach with the periodic Green's function evaluated on the basis of the Ewald transform [Ewald, 1921; Jordan et al., 1986; Eibert et al., 1999]. This is essential for implementing AIM into the periodic FE/BI formulation since the spatial domain Green's function representation is required within the AIM algorithm.

### 3. Finite Element/Fast Integral Methods

The FE/BI system (1) is partly sparse and partly dense. More specifically,  $[\mathcal{A}]$  is sparse, whereas  $[\mathcal{B}]$  is dense. Thus, although  $[\mathcal{B}]$  is typically much smaller in rank than  $[\mathcal{A}]$ , it is usually responsible for most of the CPU and memory requirements when an iterative algorithm is used for the solution of (1). Fast integral methods aim to perform the matrix-vector product  $[\mathcal{B}]\{E^S\}$  substantially faster and using less memory. For periodic problems the savings in ma-

trix fill time are especially significant when employing fast methods. In the following, AIM is applied for the solution of infinite periodic problems and FMM is used to increase the efficiency of the hybrid FE/BI method as applied to finite arrays possibly on curved platforms. A main feature of AIM and FMM is the decomposition of the BI matrix as

$$[\mathcal{B}] = [\mathcal{B}]^{\text{near}} + [\mathcal{B}]^{\text{far}}, \quad (6)$$

where the matrix  $[\mathcal{B}]^{\text{near}}$  contains the interactions between basis functions close to each other and  $[\mathcal{B}]^{\text{far}}$  contains the remaining far interactions. The elements of  $[\mathcal{B}]^{\text{near}}$  are evaluated as in the conventional method of moments (MOM) implementation. However, the product  $[\mathcal{B}]^{\text{far}}\{E^S\}$  is indirectly evaluated in an accelerated fashion utilizing the corresponding properties of the involved Green's function. FMM achieves its CPU reduction by grouping the far-zone unknowns and interacting their weighted contributions. In the case of AIM the CPU reduction is achieved by evaluating the far MOM interactions via introduction of an auxiliary uniform rectangular grid and exploiting the two-level Toeplitz properties of the Green's function on this grid. That is, FFT algorithms and the convolution theorem are invoked to compute the matrix-vector products in an iterative solver. An important feature of AIM is that its implementation is not affected by the pertinent Green's function as long as it has a convolutional form and is well-behaved for computing far-field interactions. Therefore AIM can directly be applied to periodic Green's functions. In contrast, FMM is based on a series expansion of the free-space Green's function and its implementation is not immediately extendible to analysis of infinite periodic problems.

### 3.1. Adaptive Integral Method

From (2), the BI matrix elements in (1) are obtained from [Rao et al., 1982]

$$\begin{aligned} \mathcal{B}_{mn} &= \mathcal{B}_{mn}^{(1)} + \mathcal{B}_{mn}^{(2)} \\ &= -k^2 \iint_{S_m} \iint_{S_n} g(\mathbf{r}, \mathbf{r}') \mathbf{f}_m(\mathbf{r}) \cdot \mathbf{f}_n(\mathbf{r}') ds' ds \\ &+ \iint_{S_m} \iint_{S_n} g(\mathbf{r}, \mathbf{r}') \nabla_s \cdot \mathbf{f}_m(\mathbf{r}) \nabla_s \cdot \mathbf{f}_n(\mathbf{r}') ds' ds, \quad (7) \end{aligned}$$

where  $\mathbf{f}_n$  and  $\mathbf{f}_m$  are the source and testing basis functions, respectively, on the triangles associated with the areas  $S_n$  and  $S_m$ . Without loss of gener-

ality, in the following we consider the evaluation of  $\mathcal{B}_{mn}^{(2)}$  using AIM. We begin by defining the quantities

$$q_m(\mathbf{r}) = \nabla_s \cdot \mathbf{f}_m(\mathbf{r}), \quad q_n(\mathbf{r}') = \nabla_s \cdot \mathbf{f}_n(\mathbf{r}') \quad (8)$$

which can be used to rewrite  $\mathcal{B}_{mn}^{(2)}$  as

$$\mathcal{B}_{mn}^{(2)} = \iint_{S_m} \iint_{S_n} g(\mathbf{r}, \mathbf{r}') q_m(\mathbf{r}) q_n(\mathbf{r}') ds' ds. \quad (9)$$

Next, we introduce the auxiliary expansion

$$\begin{aligned} \sum_{i=0}^{I-1} \sum_{j=0}^{J-1} Q_{ij} \delta(x - x_0 - i\Delta x) \delta(y - y_0 - j\Delta y) &= \\ \sum_{n=1}^N Q_n \sum_{i=0}^{I-1} \sum_{j=0}^{J-1} \Lambda_{ij}^{Q,n} \delta(x - x_0 - i\Delta x) & \\ \times \delta(y - y_0 - j\Delta y) & \quad (10) \end{aligned}$$

on a uniform rectangular grid, and the subsequent step is to find the coefficients  $\Lambda_{ij}^{Q,n}$  of this auxiliary expansion so that it becomes equivalent to the original Rao-Wilton-Glisson expansion. It can be shown [Bleszynski et al., 1996; Eibert and Volakis, 1999] that an appropriate equivalence relation between the two expansions is obtained by matching the moments of the basis functions. Specifically, we impose the relation

$$\begin{aligned} \iint_{S_m} q_n(\mathbf{r})(x - x_1)^{q_1} (y - y_1)^{q_2} dS &= \\ \sum_{i=0}^{I-1} \sum_{j=0}^{J-1} \Lambda_{ij}^{Q,n} (x_0 + i\Delta x - x_1)^{q_1} & \\ \times (y_0 + j\Delta y - y_1)^{q_2}, & \quad (11) \end{aligned}$$

$q_1, q_2 = 0, \dots, \infty$ .

In a numerical implementation this relation can only be fulfilled for a finite number of moments  $q_1, q_2$  and is evaluated for indices  $i = (i_n - \Delta i_1), \dots, (i_n + \Delta i_2)$  and  $j = (j_n - \Delta j_1), \dots, (j_n + \Delta j_2)$ , where  $i_n$  and  $j_n$  are the indices of the uniform grid which is closest to the center  $x_1, y_1$  of the  $n$ th edge and  $\Delta i_1, \Delta i_2, \Delta j_1, \Delta j_2$  depend on the number of moments. When (11) is substituted in (9), we obtain

$$\begin{aligned} \mathcal{B}_{mn}^{(2)} \approx \sum_{i=(i_m-\Delta i_1)}^{(i_m+\Delta i_2)} \sum_{j=(j_m-\Delta j_1)}^{(j_m+\Delta j_2)} \sum_{k=(k_m-\Delta k_1)}^{(k_m+\Delta k_2)} \sum_{l=(l_m-\Delta l_1)}^{(l_m+\Delta l_2)} & \\ \Lambda_{ki}^{Q,n} g((i\Delta x, j\Delta y), (k\Delta x, l\Delta y)) \Lambda_{ij}^{Q,m}. & \quad (12) \end{aligned}$$

In matrix form we can rewrite this as

$$[\mathcal{B}]^{(2)} \approx [\Lambda]_Q [g] [\Lambda]_Q^T = [\mathcal{B}]_{\text{AIM}}^{(2)}. \quad (13)$$

This represents a matrix product of the two sparse  $\Lambda$  matrices and the fully populated Green's function matrix  $[g]$ , which is a two-level Toeplitz matrix. The submatrix  $\mathcal{B}_{mn}^{(1)}$  in (7) can be evaluated in a manner similar to  $\mathcal{B}_{mn}^{(2)}$  except that the  $x$  and  $y$  components of the vector expansion functions must now be considered separately [Bleszynski et al., 1996; Eibert and Volakis, 1999]. The final matrix  $[\mathcal{B}]_{\text{AIM}}$  can be decomposed as

$$[\mathcal{B}]_{\text{AIM}} = [\mathcal{B}]_{\text{AIM}}^{\text{near}} + [\mathcal{B}]_{\text{AIM}}^{\text{far}} \quad (14)$$

and when this is combined with (6), we can rewrite the original  $\mathcal{B}$  matrix as

$$[\mathcal{B}]^{\text{approx}} = ([\mathcal{B}]^{\text{near}} - [\mathcal{B}]_{\text{AIM}}^{\text{near}}) + [\mathcal{B}]_{\text{AIM}}. \quad (15)$$

This expression is sort of artificial. However, it is essential to consider  $[\mathcal{B}]_{\text{AIM}}^{\text{near}}$  together with  $[\mathcal{B}]_{\text{AIM}}$  since an efficient handling is only possible for these two matrices but not for  $[\mathcal{B}]_{\text{AIM}}^{\text{far}}$ . With the representation (15) the near-zone BI interactions are evaluated without compromise in accuracy. However, since the majority of  $[\mathcal{B}]^{\text{approx}}$  consists of the Toeplitz kernel  $[g]$ , the associated matrix-vector products can be performed using only  $\mathcal{O}(N)$  memory and  $\mathcal{O}(N \log N)$  CPU time. In the final numerical implementation a near-zone threshold is defined so that  $[\mathcal{B}]^{\text{approx}}$  is a sufficiently accurate representation of  $[\mathcal{B}]$ . The threshold distance is mostly controlled by the quasi-static singularities of the Green's function. In the case of the infinite periodic Green's function, we must also account for image singularities in the neighboring periodic cells since they can be close to the test subdomains in the unit cell.

For the calculation of matrix-vector products in an iterative solver,  $[\mathcal{B}]_{\text{AIM}}$  is not computed explicitly. After mapping the actual source distributions onto the uniform grid through the  $\Lambda$  matrices, we need to only calculate the product  $[g]\{s\}$ , where  $\{s\}$  is the search vector in the iterative solver defined on the uniform grid. For a rapid computation of the product we use the FFT [Volakis et al., 1998]. Since  $[g]$  is Toeplitz/circulant, basically the product  $[g]\{s\}$  is rewritten as

$$\begin{aligned} [g]\{s\} &= \{g(i\Delta x, j\Delta y)\} * * \{s_{ij}\} \\ &= \mathcal{F}^{-1}(\mathcal{F}(\{g(i\Delta x, j\Delta y)\}) \bullet \mathcal{F}(\{s_{ij}\})), \end{aligned} \quad (16)$$

where the asterisks denote two-dimensional discrete convolution, the center dot indicates a Hadamard (e.g., term-by-term) product, and  $\mathcal{F}$  denotes discrete Fourier transform (DFT). That is, the pertinent matrix-vector products can be performed in the DFT domain using an FFT algorithm for the corresponding transformations. The speedup of AIM is due to the  $\mathcal{O}(N \log N)$  CPU requirement of the FFT algorithm. After transformation of the results back to the spatial domain, the fields on the original mesh are obtained by reverse mapping between the auxiliary unknowns and the original grid unknowns. However, for the explicit computation of  $[\mathcal{B}]_{\text{AIM}}^{\text{near}}$ , it is essential to utilize the discrete convolution representation in (16) and calculate the individual matrix elements without any Fourier transformations. If the DFT representation in (16) would be used for this step, a complexity of  $\mathcal{O}(N^2 \log N)$  would result since for each column of  $[\mathcal{B}]_{\text{AIM}}^{\text{near}}$  a complete FFT,  $\text{FFT}^{-1}$  cycle needs to be performed. This would lead to an algorithm which is worse than a conventional MOM implementation with its  $\mathcal{O}(N^2)$  complexity for matrix fill. On the other hand, only  $N$  discrete convolutions with a constant number of operations corresponding to the  $N$  elements in  $[\mathcal{B}]_{\text{AIM}}^{\text{near}}$  need to be carried out.

### 3.2. Fast Multipole Method

The FMM [Coifman et al., 1993; Bindiganavale and Volakis, 1997; Lu and Jin, 1996; Chew et al., 1997] is based on a spherical multipole and subsequent plane wave expansion of the free-space Green's function appearing in moment matrix elements as

$$\begin{aligned} \frac{e^{-jk|\mathbf{r}+\mathbf{d}|}}{|\mathbf{r}+\mathbf{d}|} &= \frac{-jk}{4\pi} \int d^2\hat{\mathbf{k}} e^{-j\mathbf{k}\cdot\mathbf{d}} \\ &\times \sum_{l=0}^{\infty} (-j)^l (2l+1) h_l^{(2)}(kr) P_l(\hat{\mathbf{k}} \cdot \hat{\mathbf{r}}). \end{aligned} \quad (17)$$

Here  $j_l$  is the spherical Bessel function,  $h_l^{(2)}$  is the spherical Hankel function of the second kind,  $P_l$  is the Legendre polynomial, and  $d < r$  is the condition for the validity of the expansion. As in the geometrical construction in Figure 2,  $\mathbf{d}$  should be kept small compared with  $\mathbf{r}$  so that the indirect evaluation of

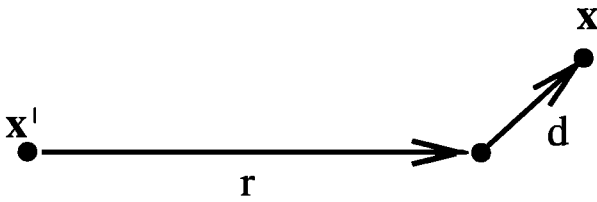


Figure 2. Geometry construction used in fast multipole method formulations.

the Green's function in (17) converges with a small number of terms kept in the multipole sum.

Following the steps given by *Coifman et al.* [1993], a matrix element can be written as

$$B_{ij} \approx \frac{-jk^3}{8\pi} \int d^2\hat{k} \mathbf{V}_{fmj}(\hat{k}) \times T_L(kr_{mm'}, \hat{k} \cdot \hat{r}_{mm'}) \mathbf{V}_{sm'i}^*(\hat{k}), \quad (18)$$

with

$$\begin{aligned} \mathbf{V}_{sm'i}(\hat{k}) &= \int_S ds' e^{-j\mathbf{k} \cdot \mathbf{r}_{i,m'}} [\bar{\mathbf{I}} - \hat{k}\hat{k}] \cdot \mathbf{f}_i(\mathbf{r}_i), \\ \mathbf{V}_{fmj}(\hat{k}) &= \int_S ds e^{-j\mathbf{k} \cdot \mathbf{r}_{j,m}} [\bar{\mathbf{I}} - \hat{k}\hat{k}] \cdot \mathbf{f}_j(\mathbf{r}_j) \end{aligned} \quad (19)$$

where  $\mathbf{f}_{i,j}(\mathbf{r}_j)$  are the basis and testing functions,  $\mathbf{k}$  is the wave vector for plane wave expansion, the asterisk denotes complex conjugation, and

$$T_L(kr, \hat{k} \cdot \hat{r}) = \sum_{l=0}^L (-j)^l (2l+1) h_l^{(2)}(kr) P_l(\hat{k} \cdot \hat{r}). \quad (20)$$

The speedup of FMM is derived from the observation that the sum in (20) is independent of  $kd$  and thus can be computed for various values of  $kr$  which can be reused, thus eliminating the need for recomputation of the time-consuming sum. To make use of the multipole expansion of the Green's function, the unknowns are grouped into clusters and the same  $T_L$  is used for the computation of the interaction between unknowns in the same cluster pairs when the clusters are far from each other.

An important parameter which affects the accuracy of the FMM implementation is the number of terms kept in the multipole expansion in the translation operator in (20). This parameter, referred to as  $L$ , is chosen here as [*Coifman et al.*, 1993]

$$L = kD_{\max} + 1.5 \log(kD_{\max} + \pi) \quad (21)$$

where  $k$  is the wave number and  $D_{\max}$  is the maximum physical size of the clusters. For this choice of  $L$ , very good accuracy (much less than 1 dB) was obtained for the analyzed array geometries. Since large values of  $L$  correspond to large CPU requirements for the FMM, it is desirable to keep  $L$  as small as possible. Clearly, for small  $L$  (less than 4) the numerical errors in evaluating the translation operators between the clusters may be unacceptable. Also, for problems involving poorly conditioned systems, iterative solutions may not converge without preconditioning. The near-field matrix (not approximated by FMM) can be used as a preconditioner in the iterative solver to improve convergence behavior. The near-field matrix involves the interactions of elements within a single cluster and additional element-to-element interactions which belong in different nearby clusters satisfying the criteria

$$d_{ij} < 1.5(r_i + r_j) \quad (22)$$

or

$$kd_{ij} < L \quad (23)$$

where  $d_{ij}$  is the separation between the centers of clusters  $i$  and  $j$  and  $r_i, r_j$  denote the radii of the clusters. It should be noted that although keeping  $L$  small decreases the FMM computations in the matrix-vector product, this also results in increased near-field matrix computations and storage as dictated by (23). Hence the designed FMM solver should be properly optimized to achieve minimum computation time within tolerable solution accuracy.

Assuming that the computational domain is divided into  $M$  groups, the total memory storage needed is  $\mathcal{O}(N^2/M) + \mathcal{O}(KN) + \mathcal{O}(KLM^2)$ , where  $K$  is the number of plane wave directions used in the numerical evaluation of the outermost integral in (18) [*Coifman et al.*, 1993]. Using the proportionalities  $K \propto L^2$ ,  $D^2 \propto N/M$ , and  $L \propto D$ , this expression can be simplified to  $C_1(N^2/M) + C_2(NM\sqrt{N/M})$ , where  $C_1$  and  $C_2$  are machine (and implementation) dependent constants. The coefficient  $C_2$  is actually quite small compared with  $C_1$ , and thus the memory is dominated by the  $\mathcal{O}(N^2/M)$  term. The CPU requirement of this FMM implementation is  $\mathcal{O}(NM) + \mathcal{O}(N^2/M)$  [*Chew et al.*, 1997; *Bindiganavale and Volakis*, 1997]. This can be minimized by choosing  $M = \sqrt{N}$ , and this results in an  $\mathcal{O}(N^{1.5})$  algorithm. The required memory for the FMM then

becomes  $\mathcal{O}(N^{1.5})$ . In practice, both the operation cost and memory requirements of FMM are less than those of standard MOM formulations for problem sizes larger than about 1000, making FMM more suitable for the solution of large problems.

## 4. Applications and Results

In this section we consider examples of infinite and finite array/FSS applications. For the infinite array examples, both commensurate and noncommensurate configurations are analyzed. Both of these involve large hybrid systems and complex configurations where the vertical periodic boundary is nonplanar for the noncommensurate case. This type of simulation for noncommensurate FSS is a new and unique capability in the context of periodic FE simulations.

### 4.1. Infinite Periodic Structures

As an example for infinite periodic structures, we consider the FSS array depicted in Figure 3. This array of slot-coupled microstrip patches was investigated by *Pous and Pozar* [1991] and acts as a strongly resonant band-pass structure. Because of its resonant characteristics, modeling of the fields between the patches with a local technique such as the FE method is a difficult task, and the mesh density must be relatively high. Also, it is noted that the in-

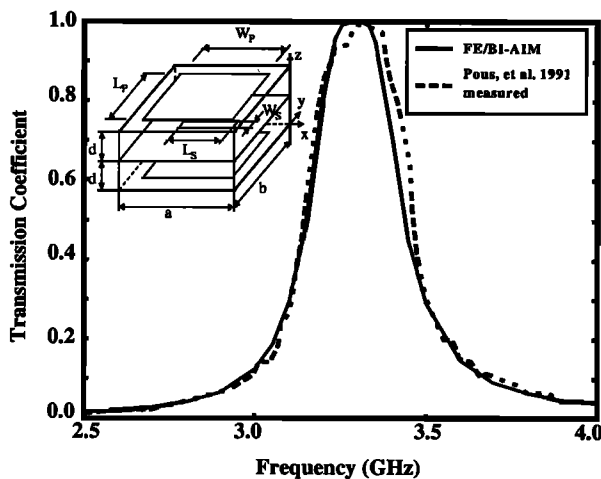


**Figure 3.** Transverse electric field transmission coefficient of slot-coupled microstrip patches compared with measured results from *Pous and Pozar*, [1991];  $\varphi = 0^\circ$  and  $\vartheta_0$  varies from  $57^\circ$  to  $32^\circ$  according to the waveguide measurement setup of *Pous and Pozar*, [1991].

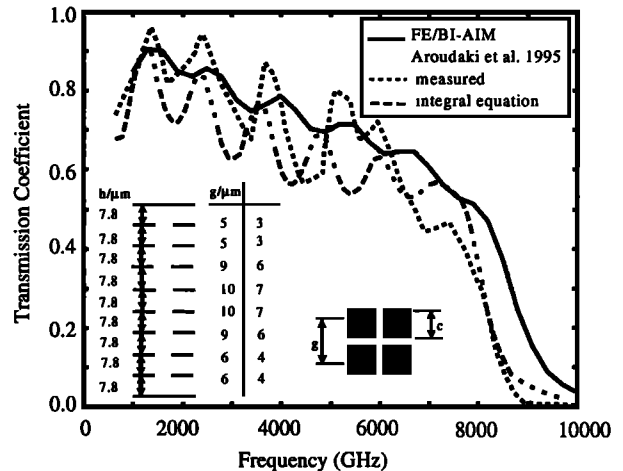


**Figure 4.** Transverse magnetic field transmission coefficient of an eight-layer frequency selective surface with noncommensurate periodicities ( $\epsilon_r = 2.3 - j0.08$ ,  $\vartheta_0 = 30^\circ$ , and  $\varphi_0 = 0^\circ$ ).

cidence angle  $\vartheta_0$  of the transverse electric (TE) plane wave varies with frequency according to the waveguide measurement setup given by *Pous and Pozar* [1991]. The curves in Figure 3 compare the transmission coefficients obtained by FE/BI AIM with measured data presented by *Pous and Pozar* [1991]. The agreement of the results is quite good. Besides the FE/BI AIM simulations, we also carried out FE/BI calculations without AIM acceleration. The results were omitted from the diagram since with proper adjustment of the AIM parameters (uniform grid density and near-zone threshold) no differences between the FE/BI and the FE/BI AIM results are encountered. With respect to complexity, both the FE/BI AIM and the FE/BI solutions used 98,636 volume and 5308 BI unknowns in each of the top and bottom BI surfaces. The simulations were run on a SUN Ultra 30 workstation. The CPU times for the frequency 3.0 GHz were 508 and 155 min for the FE/BI and the FE/BI AIM solutions, respectively, whereas the numbers of elements in the system matrix were  $55.3 \times 10^6$  and  $3.7 \times 10^6$  (equivalent to about 660 Mbyte and 45 Mbyte for 12 bytes per element). That is, AIM resulted in a memory reduction by a factor of 15 and a CPU reduction by a factor of 3.25.

Another example is the FSS low-pass filter with noncommensurate layer periodicities shown in Figure 4. This was also analyzed by *Aroudaki et al.* [1995]. The geometry consists of eight layers of

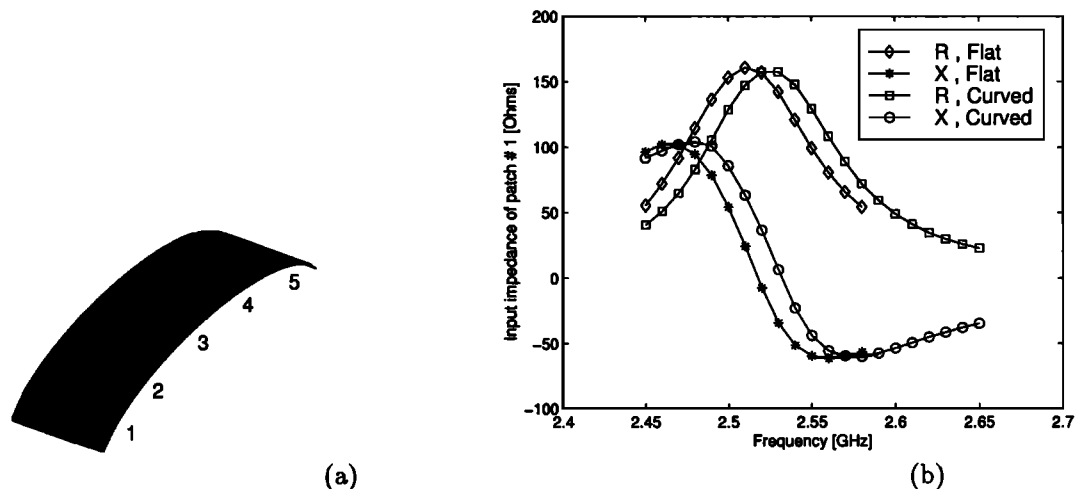


**Figure 5.** (a) Curved patch array geometry, and (b) input impedance for patch element 1 (radius of curvature = 20 cm).

square patch arrays with patch side lengths  $c$  and periods  $g$  according to the figure, which are embedded in a homogeneous dielectric ( $\epsilon_r = 2.3 - j0.08$ ). The separations between the layers are constant  $7.8 \times 10^{-6}$  m. For this problem we used an FE/BI AIM model that approximately accounts for the different periods within the structure. For the FE model the discretized unit cell just follows the varying periodicities through the height of the whole structure. The FE unknowns at the introduced steps between layers with different periods are related to corresponding edges inside the unit cell mesh by using the smaller of the two neighboring periods. The involved approximations force the fields to obey the geometric periodicities within each layer, even though this assumption may not be absolutely correct when strong coupling exists between adjacent elements. Transverse magnetic (TM) transmission curves for an incident angle  $\vartheta_0 = 30^\circ$  are compared with measured and calculated results from *Aroudaki et al.* [1995] and show pretty good agreement. Again, FE/BI and FE/BI AIM results do agree exactly if the AIM parameters are chosen appropriately.

#### 4.2. Finite Arrays

The greatest advantage of the FMM implementation is its capability for an efficient computation of three-dimensional (3-D) problems. The necessity of using 3-D FFTs in AIM implementations may not render AIM as attractive without suitable optimiza-

tions on the implementation of the FFT. Thus, for doubly curved arrays we consider implementation of the FE/BI methods with FMM rather than AIM. Currently, the half-space Green's function is used as an approximation for slightly curved BI terminations. Below we show some results for the analysis of a five-element patch array on a curved surface. The geometry is illustrated in Figure 5a. The effect of curvature on the radiation pattern and the input impedance of the antenna elements are examined using the FE/BI FMM approach. For flat arrays, each antenna element is a rectangular patch of size  $3.5 \times 2.625$  cm, and we consider two different center-to-center spacings, 6.125 and 5.250 cm. The flat arrays are backed by rectangular cavities of dimensions  $33.25 \times 6.125 \times 0.3175$  cm and  $28.00 \times 6.125 \times 0.3175$  cm, respectively, and are recessed in an infinite metallic ground plane. The cavities are filled with a material of relative permittivity 2.32, and curved arrays are formed from the flat by wrapping them onto metallic circular cylindrical platforms of radius 20 cm (spacing 6.125 cm) or 10 cm (spacing 5.250 cm). For both arrays the five patches are fed inphase by an offset vertical probe of constant current. A typical surface mesh (discretization into squares of dimensions  $0.4375 \times 0.4375$  cm and subsequent division into triangles) is given in Figure 5a for the curved array with spacing 6.125 cm.

Figure 5b and Figures 6a and 6b show the dependence on curvature of the input impedance of the

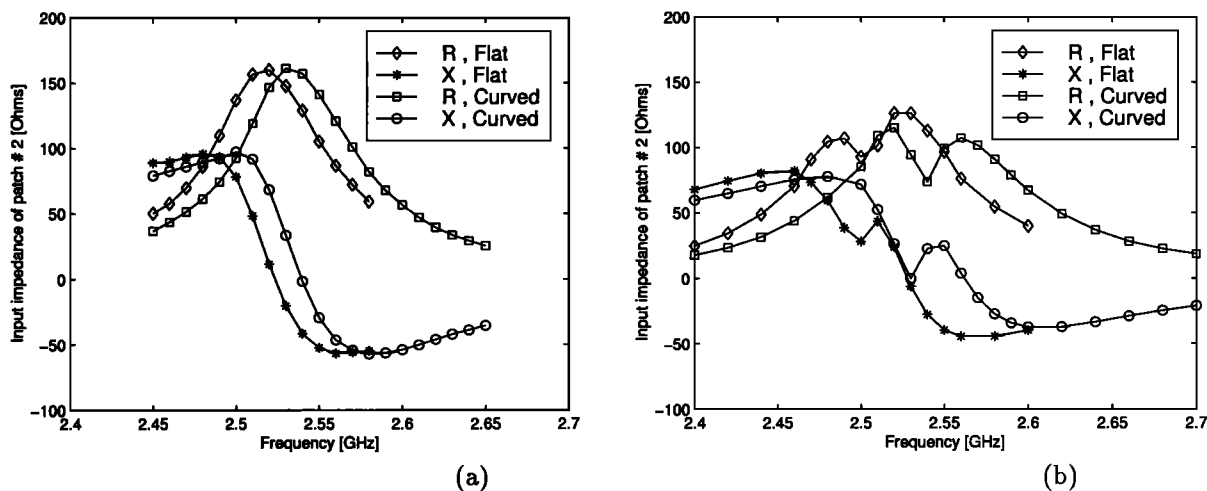


**Figure 6.** (a) Input impedance for patch element 2 (radius of curvature = 20 cm), and (b) input impedance for patch element 2 (radius of curvature = 10 cm).

first and second array element for flat and curved array geometries. This is shown for the two different element spacings of 6.125 and 5.250 cm. The effect of coupling is observed clearly for the input impedance of the second element when the spacing between the elements is 5.250 cm. The odd-numbered array elements show a similar behavior for both curvatures, whereas the even-numbered elements suffer coupling as the platform curvature is increased due to the excited surface waves.

## 5. Conclusions

In this paper we discussed the application of fast integral methods to hybrid FE/BI modeling of conformal antenna and array problems. AIM was chosen for planar BI termination surfaces since only two-dimensional FFTs need be performed in this case. Also, periodic Green's functions can be included in a straightforward manner because AIM makes use only of the convolutional properties of the Green's function. On the other hand, the concept of FMM is more favorable for nonplanar termination surfaces. Both AIM and FMM realize their speedups through an efficient computation of the BI far interactions. However, since they keep the conventional BI formulation for the near-coupling terms, they can produce results without compromise in accuracy. Implementation issues related to AIM and FMM were discussed, and application results were given which

demonstrate the practicability and efficiency of the approaches for large-scale and broadband computations.

## References

- Anastassiou, H. T., M. Smelyanskiy, S. S. Bindiganavale, and J. L. Volakis, Scattering from relatively flat surfaces using the adaptive integral method, *Radio Sci.* **33**(1), 7–16, 1998.
- Aroudaki, H., V. Hansen, H.-P. Gemünd, and E. Kreysa, Analysis of low-pass filters consisting of multiple stacked FSSs of different periodicities with applications in the submillimeter radioastronomy, *IEEE Trans. Antennas Propag.* **43**(12), 1486–1491, 1995.
- Bindiganavale, S. S., and J. L. Volakis, Comparison of three FMM techniques for solving hybrid FE/BI systems, *IEEE Antennas Propag. Mag.* **39**(4), 47–59, 1997.
- Bindiganavale, S. S., and J. L. Volakis, Scattering and radiation from planar structures containing small features using a finite element fast integral method, *Electron. Lett.* **34**(21), 2015–2016, 1998.
- Bleszynski, E., M. Bleszynski, and T. Jaroszewicz, AIM: Adaptive integral method for solving large-scale electromagnetic scattering and radiation problems, *Radio Sci.* **31**(5), 1225–1251, 1996.
- Bojarski, N. N., K-space formulation of the electromagnetic scattering problem, *Tech. Rep. AFAL-TR-71-5*, U.S. Air Force, March 1971.
- Burkholder, R. J., and D. H. Kwon, High-frequency asymptotic acceleration of the fast multipole method, *Radio Sci.* **31**(5), pp. 1199–1206, 1996.
- Chew, W. C., J. Jin, C. Lu, E. Michielssen, and J.

- M. Song, Fast solution methods in electromagnetics, *IEEE Trans. Antennas Propag.* 45(3), 533–543, 1997.
- Coifman, R., V. Rokhlin, and S. Wandzura, The fast multipole method for the wave equation: A pedestrian prescription, *IEEE Antennas Propag. Mag.* 35(3), 7–12, 1993.
- Eibert, T. F., J. L. Volakis, D. R. Wilton, and D. R. Jackson, Hybrid FE/BI modeling of 3D doubly periodic structures utilizing triangular prismatic elements and a MPIE formulation accelerated by the Ewald transformation, *IEEE Trans. Antennas Propag.*, in press, 1999.
- Eibert, T. F., and J. L. Volakis, Adaptive integral method for hybrid FE/BI modeling of 3D doubly periodic structures, *IEE Proc. Microwaves, Antennas Propag.* 146, 17–22, Feb. 1999.
- Ewald, P. P., Die Berechnung optischer und elektrostatischer Gitterpotentiale, *Ann. Phys.* 64, 253–268, 1921.
- Graglia, R. D., D. R. Wilton, A. F. Peterson, and I.-L. Gheorma, Higher order interpolatory vector bases on prism elements, *IEEE Trans. Antennas Propag.* 46(3), 442–450, 1998.
- Jordan, K. E., G. R. Richter, and P. Sheng, An efficient numerical evaluation of the Green's function for the Helmholtz operator on periodic structures, *J. Comput. Phys.* 43, 222–235, 1986.
- Lu, N., and J.-M. Jin, Application of the fast multipole method to finite-element boundary-integral solution of scattering problems, *IEEE Trans. Antennas Propag.* 44(6), 781–786, 1996.
- Lucas, E. W., and T. W. Fontana, A 3-D hybrid finite element/boundary element method for the unified radiation and scattering analysis of general infinite periodic arrays, *IEEE Trans. Antennas Propag.* 43(2), 145–153, 1995.
- McGrath, D. T., and V. P. Pyati, Periodic structure analysis using a hybrid finite element method, *Radio Sci.* 31(5), 1173–1179, 1996.
- Özdemir, T., and J. L. Volakis, Triangular prisms for edge-based vector finite elements analysis, *IEEE Trans. Antennas Propag.* 45(5), 788–797, 1997.
- Pous, R., and D. M. Pozar, A frequency-selective surface using aperture-coupled microstrip patches, *IEEE Trans. Antennas Propag.* 39(12), 1763–1769, 1991.
- Rao, S. M., D. R. Wilton, and A. W. Glisson, Electromagnetic scattering by surfaces of arbitrary shape, *IEEE Trans. Antennas Propag.* 30(3), 409–418, 1982.
- Saad, Y., *Iterative Methods for Sparse Linear Systems*, PWS, Boston, Mass. 1996.
- Sheng, X. Q., J.-M. Jin, J. M. Song, C. C. Lu, and W. C. Chew, On the formulation of hybrid finite-element and boundary-integral methods for 3-D scattering, *IEEE Trans. Antennas Propag.* 46(3), 303–311, 1998.
- Song, J. M., C. C. Lu, and W. C. Chew, Multilevel fast multipole algorithm for electromagnetic scattering by large complex objects, *IEEE Trans. Antennas Propag.* 45(10), 1488–1493, 1997.
- Volakis, J. L., T. Özdemir, and J. Gong, Hybrid finite element methodologies for antennas and scattering, *IEEE Trans. Antennas Propag.* 45(3), 493–507, 1997.
- Volakis, J. L., A. Chatterjee, and L. C. Kempel, *Finite Element Methods for Electromagnetics*, IEEE Press, Piscataway, N.J., 1998.

---

T. F. Eibert, K. Sertel, and J. L. Volakis, Radiation Laboratory, Department of Electrical Engineering and Computer Science, University of Michigan, 1301 Beal Avenue, Ann Arbor, MI 48104-2212. (volakis@eecs.umich.edu)

(Received January 26, 1999; revised April 20, 1999; accepted April 26, 1999.)